Unusual {···HNC_2O···HC_nO}, n = 1 or 2, synthons predominate in the molecular packing of the one-dimensional coordination polymers, {$Cd[S_2P(OR)_2]_2(^3LH_2)\}_n$, for *R* = Me and Et, but are precluded when *R* = *i*-Pr; $^3LH_2$ = *N*,*N*′-bis(3-pyridylmethyl)oxalamide†

Yee Seng Tan,[a] Chien Ing Yeo,[a] Huey Chong Kwong[a] and Edward R. T. Tiekink[a,*]

Research Centre for Crystalline Materials, School of Medical and Life Sciences, Sunway University, 47500 Bandar Sunway, Selangor Darul Ehsan, Malaysia

E-mail: edwardt@sunway.edu.my (ERTT)

ORCID ID: 0000-0002-0144-3298 (YST); 0000-0002-3224-3782 (CIY); 0000-0001-5130-8011 (HCK); 0000-0003-1401-1520 (ERTT)

Abstract

Linear, one-dimensional coordination polymers, {$Cd[S_2P(OR)_2]_2(^3LH_2)\}_n$, for *R* = Me (**1**), Et (**2**) and *i*-Pr (**3**) have been fully characterised by a variety of physiochemical, spectroscopic, crystallographic and computational techniques. Two-dimensional layers are apparent in the crystals of **1** and **2**, being mediated, respectively, by unusual {···HNC_2O···HC_nO}, n = 1 or 2, synthons formed between the oxalamide and phosphorus-bound alkoxy residues. Related synthons are not observed in the crystal of **3**, with supramolecular tapes, mediated by concatenated {···$HNC_2O\}_2$ synthons, being formed instead. The observed differences in supramolecular association are ascribed to the increased steric bulk and reduced inductive effect of the *R* = *i*-Pr group compared with *R* = Me and Et.

Footnote

† Electronic supplementary information (ESI) available: PXRD patterns, NMR spectra, d_{norm}-Hirshfeld surface diagrams and fingerprint plots. CCDC 2145322-2145324 contain the supplementary crystallographic data for this paper. For ESI and crystallographic data in CIF or other electronic format see DOI: 10.1039/d0cexxxxxx

Introduction

Featuring di-amide and pyridyl functionality, the flexible *N*,*N*′-bis(3-pyridylmethyl)oxalamide molecule ($^3LH_2$), Fig. 1, and the 2- and 4- isomeric forms, along with their sulphur analogues, present many prospects for the rational design of tailored aggregates in crystals. Thus, the presence of the central oxalamide moiety offers opportunities for the formation of supramolecular tapes[1] while pyridyl-N atoms are highly prone to associate with different organic residues such as carboxylic acids[2] and are ideal for coordination to a wide variety of metal centres.[3] As highlighted in a recent bibliographic review,[4] all of these possibilities have been realised although studies with these molecules are relatively limited in consideration of the supramolecular association opportunities patently available and in recognition of their relatively straightforward synthesis.[5,6]

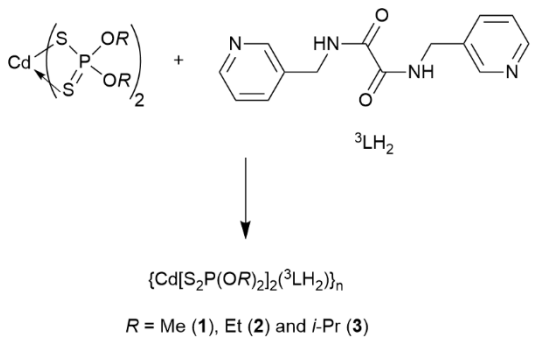

Fig. 1 Outline for the reaction of $Cd[S_2P(OR)_2]_2$ and $^3LH_2$ yielding $\{Cd[S_2P(OR)_2]_2(^3LH_2)\}_n$ for *R* = Me (**1**), Et (**2**) and *i*-Pr (**3**).

A highlight from the (relatively) early literature of $^nLH_2$ is the assembly of $^3LH_2$ and N,N'-dicarboxymethylurea molecules into a two-dimensional array in a 1:1 co-crystal through a combination of 10-membered amide synthons, $\{\cdots HNC_2O\}_2$, and six-membered {···O···HNCNH} synthons, respectively, with the connections between the parallel tapes being of the type carboxylic acid-O–H···N(pyridyl).[7] The $^nLH_2$ molecules also featured in early systematic studies in halogen bonding.[4] For example, the 1:1 co-crystal formed between $^3LH_2$ and 1,4-di-iodobuta-1,3-diyne, features supramolecular tapes formed by $^3LH_2$, mediated by 10-membered amide $\{\cdots HNC_2O\}_2$ synthons, being cross-linked by I···N halogen bonding within a two-dimensional array.[8] In terms of interacting with metal centres, $^3LH_2$, for example, has been shown to bridge two $Zn[S_2CN(Me)CH_2CH_2OH]_2$ molecules *via* Zn–N(pyridyl) dative bonding, which, through conventional hydroxyl-O–H···O(hydroxyl) hydrogen bonding, was assembled to interwoven double chains.[9] The other notable feature of the $^nLH_2$ molecules is their conformational flexibility as seen in the polymorphs of the n = 3[10] and 4[11,12] isomers; computational chemistry indicates the energy differences between the opposing *syn*-periplanar and *anti*-periplanar conformations for $^nLH_2$ and their sulphur analogues is a matter of 4-8 kJ mol^{-1}.[10,13]

In continuation of on-going structural studies designed to increase the dimensionality of supramolecular aggregates of the zinc-triad 1,1-dithiolates,[14,15] *e.g.* 1,1-dithiolate = dithiocarbamate ($^-S_2CNR_2$), xanthate (^-S_2COR) and dithiophosphate [$^-S_2P(OR)_2$], through the complexation of bridging bipyridyl-type ligands,[16] *N*,*N*′-bis(*n*-pyridylmethyl)oxalamide ligands have been investigated, owing to their coordinating ability towards metal ions and

capacity to further self-assemble through hydrogen bonding.[17-20] In systematic studies of coordination polymer formation mediated by zinc and cadmium bis(dithiophosphate) and bipyridyl-type molecules, a clear influence of the dithiophosphate-bound *R* group upon the dimensionality of the resulting aggregate was noted. This is nicely exemplified by the structure of the one-dimensional coordination polymer formed by $\{Zn[S_2P(O\text{-}i\text{-}Pr)_2]_2(4,4'\text{-bipyridyl})\}_n$ (ref. 21) which could be isolated for the relatively small *R* = *i*-Pr group but when the steric bulk of the dithiophosphate-*R* group was increased to cyclohexyl (Cy) only the zero-dimensional binuclear species could be isolated, *viz*. $\{Zn[S_2P(OCy)_2]_2\}_2(4,4'\text{-bipyridyl})$.[22] A similar situation pertains in the pair of cadmium dithiophosphate structures complexed to *trans*-1,2-bis(4-pyridyl)propane: for *R* = *i*-Pr a one-dimensional coordination is generated in the crystal but a binuclear species is formed for *R* = Cy despite both cadmium atom coordination geometries are based on *cis*-N_2S_4 donor sets.[23] Herein, in continuation of recent studies,[24-26] three cadmium bis(dithiophosphate) species of $^3LH_2$ are investigated in order increase the amount of supramolecular association, through conventional hydrogen bonding, between the anticipated one-dimensional coordination polymers.

Experimental

Chemicals and instrumentation

All chemicals and solvents were used as purchased without purification. The melting points were determined on a Stuart melting point apparatus SMP30. Elemental analyses were performed on a Leco TruSpec Micro CHN Elemental Analyser. The IR spectra were measured on a Bruker Vertex 70v FTIR spectrophotometer from 4000 to 80 cm^{-1}; abbreviations: *s*, strong; *m*, medium; *w*, weak. The ^1H and $^{13}C\{^1H\}$ NMR spectra were recorded in DMSO-d_6 solutions on a Bruker Ascend 400 MHz NMR spectrometer with chemical shifts relative to tetramethylsilane. The $^{31}P\{^1H\}$ NMR spectra were also recorded in DMSO-d_6 solution on the

same instrument with the chemical shifts recorded relative to 85% aqueous H_3PO_4 as the external reference; abbreviations for NMR assignments: *d*, doublet; *dd*, doublet of doublets; *ddd*, doublet of doublet of doublets; *dq*, doublet of quartets; *ds*, doublet of septets; *t*, triplet; *m*, multiplet; *br*, broad. The $^{13}C\{^1H\}$ cross polarised magic angle spinning (CP MAS) spectra were recorded on a Bruker Ascend 400 MHz NMR spectrometer equipped with a PH MASVTN 400SB probe at 100.7 MHz with the sample packed in a 4 mm zirconia rotor and subjected to a MAS rate at 12 kHz. The chemical shifts were referenced to the methylene carbon of adamantane at 38.48 ppm. Powder X-ray diffraction (PXRD) measurements were performed on a Rigaku SmartLab with CuKα1 radiation (λ = 1.54060 Å) in the 2θ range 5 to 40° with a step size of 0.010°. The experimental PXRD patterns were compared to the simulated PXRD patterns calculated from the respective Crystallographic Information Files (CIFs) using the Rigaku PDXL2 structure analysis software package (https://www.rigaku.com/en/products/software/pdxl/overview).

Synthesis and characterisation of 1-3

The $Cd[S_2P(OR)_2]_2$ precursors, for *R* = Me, Et and *i*-Pr,[27] and *N*,*N*′-bis(3-pyridylmethyl)oxalamide ($^3LH_2$)[5] were prepared following literature procedures. The 1:1 adduct, $\{Cd[S_2P(OMe)_2]_2(^3LH_2)\}_n$ was obtained by mixing a suspension of $Cd[S_2P(OMe)_2]_2$ (0.50 g, 1.15 mmol) and $^3LH_2$ (0.31 g, 1.15 mmol) in dimethylformamide (Merck; 5 mL) followed by stirring for 30 min at 373 K. A milky-yellow solid precipitated upon cooling which was collected and recrystallised in absolute ethanol. Colourless prisms formed after one week. Colourless crystals of the ethyl and *i*-propyl analogues, **2** and **3**, were prepared in a similar manner.

$\{Cd[S_2P(OMe)_2]_2(^3LH_2)\}_n$ (**1**):

Yield: 0.53 g, 65%. M.pt: > 423 (dec.). Calcd for $C_{18}H_{26}CdN_4O_6P_2S_4$: C, 31.02; H, 3.76; N, 8.04. Found: C, 31.00; H, 3.85; N, 8.03%. FTIR (cm^{-1}): 1184(w) ν(C−O); 994(s) ν(P−O); 646(s) ν(P−S); 367(m) ν(Cd−N); 263(m) ν(Cd−S). ^{1}H NMR (DMSO-d_6, ppm): 9.43 (*t*, 2H, NH, J_{HH} = 6.38 Hz), 8.50 (*dd*, 2H, py-H_2, J_{HH} = 2.20, 0.57 Hz), 8.46 (*dd*, 2H, py-H_4, J_{HH} = 4.82, 1.64 Hz), 7.71–7.68 (*m*, 2H, py-H_6), 7.37 (*ddd*, 2H, py-H_5, J_{HH} = 7.82, 4.83, 0.75 Hz), 4.36 (*d*, 4H, CH_2, J_{HH} = 6.40 Hz), 3.57 (*d*, 12H, OCH_3 , J_{HP} = 14.77 Hz). ^{13}C{^{1}H} NMR (DMSO-d_6, ppm): 160.6 (C=O), 149.3 (py-C_2), 148.7 (py-C_3), 136.0 (py-C_5), 134.8 (py-C_1), 124.1 (py-C_4), 53.2 (*d*, OCH_3, J_{CP} = 6.50 Hz); the CH_2 signal was overlapped with those of the solvent. ^{31}P{^{1}H} NMR (DMSO-d_6, ppm): 115.6. ^{13}C CPMAS {25 °C}: 159.7 (C=O), 149.9 (py-$C_{2,3}$), 139.9 (py-C_5), 135.1 (py-C_1), 125.6 (py-C_4), 56.5, 54.4 (OCH_3, J_{PC} = 215.3 Hz), 41.6 (CH_2) ppm.

$\{Cd[S_2P(OEt)_2]_2(^3LH_2)\}_n$ (**2**):

Yield: 0.45 g, 58%. M.pt: >447 K (dec.). Calcd for $C_{22}H_{34}CdN_4O_6P_2S_4$: C, 35.08; H, 4.55; N, 7.44. Found: C, 35.08; H, 4.75; N, 7.40%. FTIR (cm^{-1}): 1189(w) ν(C−O); 1006(s) ν(P−O); 647(s) ν(P−S); 374(w) ν(Cd−N); 258(m) ν(Cd−S). ^{1}H NMR (DMSO-d_6, ppm): 9.44 (*t*, 2H, NH, J_{HH} = 6.38 Hz), 8.51 (*dd*, 2H, py-H_2, J_{HH} = 2.24, 0.64 Hz), 8.47 (*dd*, 2H, py-H_4, J_{HH} = 4.81, 1.64 Hz), 7.72–7.69 (*m*, 2H, py-H_6), 7.37 (*ddd*, 2H, py-H_5, J_{HH} = 7.82, 4.82, 0.75 Hz), 4.36 (*d*, 4H, CH_2, J_{HH} = 6.41 Hz), 4.02 (*dq*, 8H, OCH_2, J_{HH} = 7.07 Hz, J_{HP} = 9.68 Hz), 1.23 (*t*, 12H, CH_3, J_{HH} = 7.07 Hz). ^{13}C{^{1}H} NMR (DMSO-d_6, ppm): 160.6 (C=O), 149.3 (py-C_2), 148.7 (py-C_3), 136.0 (py-C_5), 134.8 (py-C_1), 124.1 (py-C_4), 62.5 (*d*, OCH_2, J_{CP} = 6.27 Hz), 16.4 (*d*, CH_3, J_{CP} = 8.57 Hz); the CH_2 signal was overlapped with those of the solvent. ^{31}P{^{1}H} NMR (DMSO-d_6, ppm): 110.1 ppm. ^{13}C CPMAS {25 °C}: 160.1 (C=O), 150.1 (*br*, py-C_2), 149.8 (*br*, py-C_3), 141.4 (py-C_5), 135.5 (py-C_1), 127.2 (py-C_4), 66.6, 63.6 (OCH_2, J_{PC} = 298.0 Hz), 40.8 (CH_2), 15.4 (CH_3) ppm.

$\{Cd[S_2P(O\text{-}i\text{-}Pr)_2]_2(^3LH_2)\}_n$ (**3**):

Yield: 0.36 g, 48%. M.pt: >458 K (dec.). Calcd for $C_{26}H_{42}CdN_4O_6P_2S_4$: C, 38.59; H, 5.23; N, 6.92. Found: C, 38.56; H, 5.24; N, 6.83%. FTIR (cm^{-1}): 1187(w) ν(C−O); 962(s) ν(P−O); 644(s) ν(P−S); 371(w) ν(Cd−N); 260 (m) ν(Cd−S). ^1H NMR (DMSO-d_6, ppm): 9.44 (*t*, 2H, NH, J_{HH} = 6.37 Hz), 8.51 (*dd*, 2H, py-H_2, J_{HH} = 2.28, 0.65 Hz), 8.47 (*dd*, 2H, py-H_4, J_{HH} = 4.81, 1.63 Hz), 7.71–7.68 (*m*, 2H, py-H_6), 7.37 (*ddd*, 2H, py-H_5, J_{HH} = 7.82, 4.81, 0.74 Hz), 4.81 (*ds*, 4H, OCH, J_{HH} = 6.39 Hz, J_{HP} = 12.39 Hz), 4.36 (*d*, 4H, CH_2, J_{HH} = 6.41 Hz), 1.27 (*d*, 24H, CH_3, J_{HH} = 6.21 Hz). $^{13}C\{^1H\}$ NMR (DMSO-d_6, ppm): 160.6 (C=O), 149.3 (py-C_2), 148.7 (py-C_3), 136.0 (py-C_5), 134.8 (py-C_1), 124.0 (py-C_4), 71.2 (*d*, OCH, J_{CP} = 5.55 Hz), 23.9 (*d*, CH_3, J_{CP} = 4.53 Hz); the CH_2 signal was overlapped with those of the solvent. $^{31}P\{^1H\}$ NMR (DMSO-d_6, ppm): 107.1. ^{13}C CPMAS {25 °C}: 160.6 (C=O), 151.1 (py-C_2), 149.3, 148.7 (py-C_3), 141.2, 139.1 (py-C_5), 135.7 (py-C_1), 127.1, 126.1 (py-C_4), 75.9, 74.8, 73.2, 71.9 (OCH, J_{PC} = 106.6, 130.5 Hz), 43.2 – 42.7 (*m*, *br*, CH_2), 26.8 – 23.1 (*m*, CH_3) ppm.

X-ray crystallography

Selected crystal data and refinement details for **1**-**3** are collated in Table 1. Intensity data for colourless crystals of **1** (0.05 x 0.07 x 0.17 mm), **2** (0.04 x 0.06 x 0.21 mm) and **3** (0.08 x 0.10 x 0.27 mm) were measured at 100 K on a Rigaku/Oxford Diffraction XtaLAB Synergy diffractometer (Dualflex, AtlasS2) fitted with CuKα radiation (λ = 1.54184 Å); 100% data completeness was achieved at θ = 67.1°. Data processing and Gaussian absorption corrections were accomplished with CrysAlis Pro.[28] The structures were solved by dual space direct methods using ShelXT.[29] The refinements were by full-matrix least squares (on F^2) with anisotropic displacement parameters for all non-hydrogen atoms.[30] The C-bound hydrogen atoms were included in the models in their calculated positions and the N-bound hydrogen

atoms were located from a difference map and refined with N–H = 0.88±0.01 Å. A weighting scheme of the form $w = 1/[\sigma^2(F_o^2) + (aP)^2 + bP]$, where $P = (F_o^2 + 2F_c^2)/3$, was introduced in each case. The crystallographic analysis also included the use of the programs WinGX,[31] ORTEP-3 for Windows,[31] PLATON[32] and DIAMOND.[33]

Table 1 Crystal data and refinement details for the crystals of **1**-**3**

Compound	**1**	**2**	**3**
Formula	$C_{18}H_{26}CdN_4O_6P_2S_4$	$C_{22}H_{34}CdN_4O_6P_2S_4$	$C_{26}H_{42}CdN_4O_6P_2S_4$
Molecular weight	697.01	753.11	809.21
Crystal system	triclinic	triclinic	triclinic
Space group	$P\bar{1}$	$P\bar{1}$	$P\bar{1}$
Z	1	1	2
a (Å)	7.2387(1)	9.0611(3)	9.9154(1)
b (Å)	9.6411(2)	9.2065(3)	12.3655(1)
c (Å)	10.4545(2)	10.5703(4)	15.4749(2)
α (º)	81.448(1)	82.436(3)	106.080(1)
β (º)	75.399(1)	77.672(3)	99.172(1)
γ (º)	70.165(2)	64.113(3)	91.827(1)
V (Å^3)	662.56(2)	774.27(5)	1794.03(3)
D_x (g cm^{-3})	1.747	1.615	1.498
F(000)	352	384	832
μ (mm^{-1})	11.062	9.513	8.252
no. reflections	14558	16964	38837
no. unique reflections	2373	2767	6411
no. reflections with			

$I \geq 2\sigma(I)$	2360	2752	6229
R (obs. data)	0.016	0.016	0.018
a and b in weighting scheme	0.024; 0.401	0.018; 0.429	0.025; 1.022
R_w (all data)	0.043	0.040	0.046
Max. and min. residual peaks (eÅ^{-3})	0.34; -0.35	0.31; -0.29	0.46; -0.46

Results and discussion

The facile 1:1 reaction between $Cd[S_2P(OR)_2]_2$ and *N*,*N*′-bis(3-pyridylmethyl)oxalamide ($^3LH_2$) gave rise to three one-dimensional coordination polymers: *R* = Me (**1**), Et (**2**) and *i*-Pr (**3**). Powder X-ray diffraction patterns measured at room temperature on the bulk material indicated a match to that simulated from the 100 K single crystal structure determination in each case, see ESI† Fig. 1. The infrared spectra of **1**-**3**, ESI† Fig. 2, showed strong characteristic peaks for the dialkyldithiophosphate ligands, attributed to ν(P−O) in the region 962 to 1006 cm^{-1} and ν(P−S) at approximately 645 cm^{-1}, while peaks ascribed to the ν(C−O) vibration occurred as a weak signal at ~1187 cm^{-1}. The successful complexation of cadmium(II) by the dialkyldithiophosphate and $^3LH_2$ ligands is clearly indicated by the presence of medium intensity ν(Cd−S) bands in the region 258 to 263 cm^{-1}, and ν(Cd−N) bands in the range 367 to 374 cm^{-1}.

An NMR study in DMSO-d_6 solution for each of **1**-**3** was conducted to confirm the stoichiometry of the materials and to provide additional evidence for sample purity. Thus, the ^{1}H, ^{13}C{^{1}H} and ^{31}P{^{1}H} NMR spectra exhibited the expected NMR resonances (and integration for ^{1}H spectra); original spectra are included in ESI† Figs 3-5. In the ^{1}H NMR

spectra, the NH signals of $^{3}LH_2$ are observed at ~9.43 ppm. The α-protons of the alkoxy groups exhibited coupling with the ^{31}P nuclei. Coupling induced by ^{31}P was also manifested in the $^{13}C\{^{1}H\}$ spectra. Notable also were the downfield resonances due to C=O. The absence of $^{13}C\{^{1}H\}$ methylene-C resonances in the spectra is due to their signals being masked by the DMSO-d_6 signals, an observation confirmed by the solid-state ^{13}C CPMAS NMR spectra measured for **1**-**3** (see below). In the $^{31}P\{^{1}H\}$ NMR, a singlet was observed for each of **1**-**3** with a systematic high-field shift passing from **1** to **3**, which is correlated with the relative inductive effects of the *R* groups. The absence of $^{111/113}Cd$ satellites in the $^{31}P\{^{1}H\}$ spectra confirms fast dithiophosphate exchange at the Cd centre in DMSO-d_6 solution. These results are consistent with closely related systems where no indication for the retention of the one-dimensional coordination polymer in solution was noted.[24-26]

The solid-state ^{13}C CPMAS NMR spectra were recorded at 25 °C for **1**-**3** (see ESI† Fig. 6) and that for **3** is shown in Fig. 2. The resonances due to methylene-C, not observed in the solution spectra, are evident in the range 40 to 45 ppm as two, overlapped broad resonances reflecting the presence of two independent molecules in the asymmetric-unit as indicated by the crystallographic analysis (see below). Splitting is evident for the methine-C nuclei, with two well-resolved doublets in the region 70 to 75 ppm owing to coupling with the adjacent ^{31}P nuclei. The methyl-C nuclei were resolved into a 1:1:2:2:1:1 pattern, again consistent with the crystallographic observations (see below); see insert of Fig. 2.

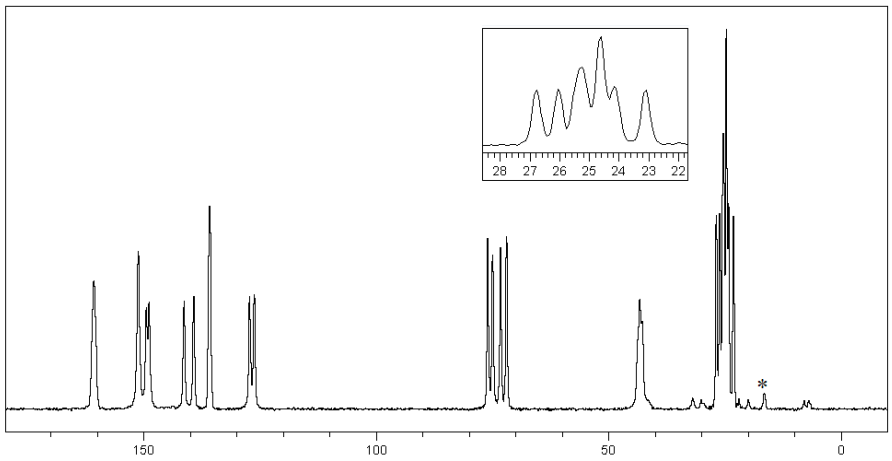

Fig. 2 The solid-state ^{13}C CP MAS spectrum of **3** measured at 25 °C. The inset shows an expanded view of the methyl-C region. " * " denotes spinning side-bands.

Molecular structures of 1-3

The crystallographic asymmetric-unit of **1** comprises half a cadmium atom, being located on a centre of inversion, a dithiophosphate anion and half a molecule of $^{3}LH_2$, this also being located about a centre of inversion. The same description of the asymmetric-unit is true for **2**. However, in **3** the asymmetric-unit is doubled but each constituent has the same symmetry as noted for **1** and **2**. The cadmium coordination geometries, as might be anticipated, closely resemble each other, each featuring a *trans*-N_2S_4 donor set, as can be seen from Fig. 3. The selected geometric parameters collated in Table 2 also reflect the similarities in the molecular structures and a lack of systematic trends. The dithiophosphate ligands are chelating effectively symmetrically in **1** (Δ(Cd–S_{long} - Cd–S_{short}) = 0.01 Å) and **3** (ΔCd–S = 0.03 Å) but form slightly disparate Cd–S bonds in the case of **2** (ΔCd–S = 0.12 Å).

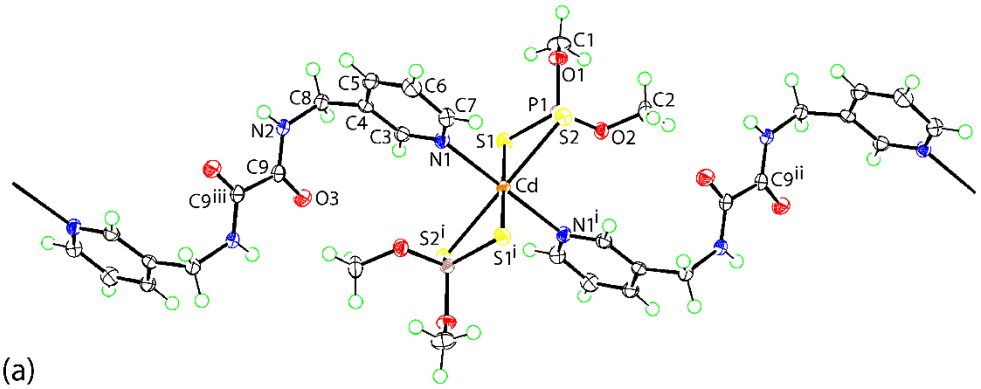
C1
O1
C5
C6
C8
C7
P1
C2
C4
C3
N2
S1
S2
O2
N1
C9
Cd
C9iii
O3
C9ii
S2i
N1i
S1i

(a)

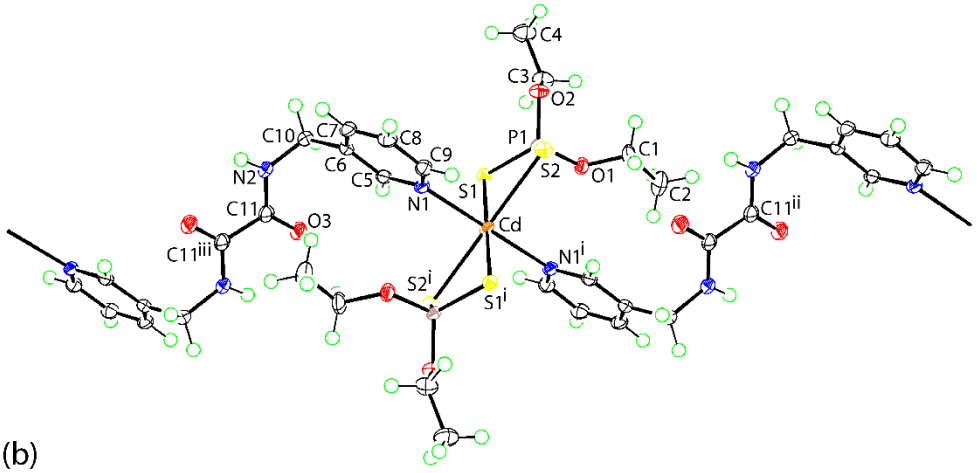
C4
C3
O2
C10
C7
C8
P1
C9
C6
N2
S2
C1
C5
S1
O1
N1
C2
C11
O3
Cd
C11ii
C11iii
N1i
S2i
S1i

(b)

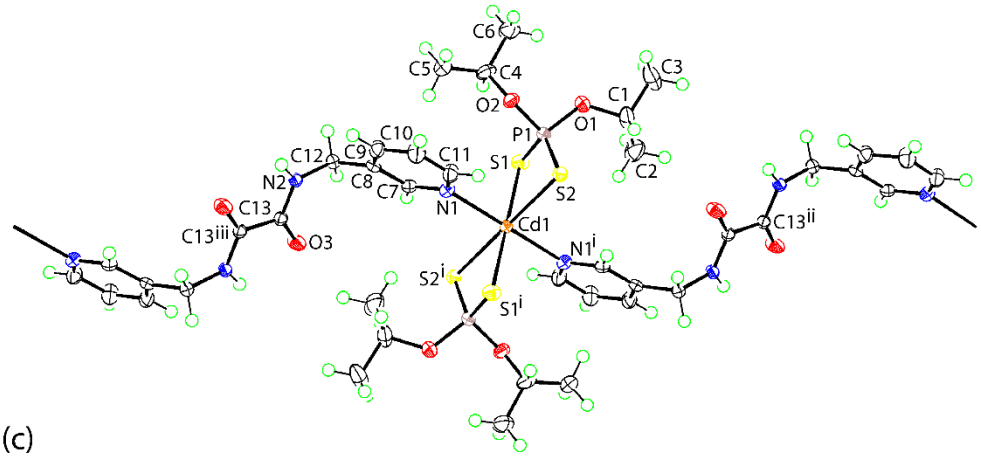
C6
C5
C4
C3
O2
C1
O1
P1
C10
C12
C9
C11
S1
C2
N2
C8
C7
S2
N1
C13
Cd1
C13ii
C13iii
O3
N1i
S2i
S1i

(c)

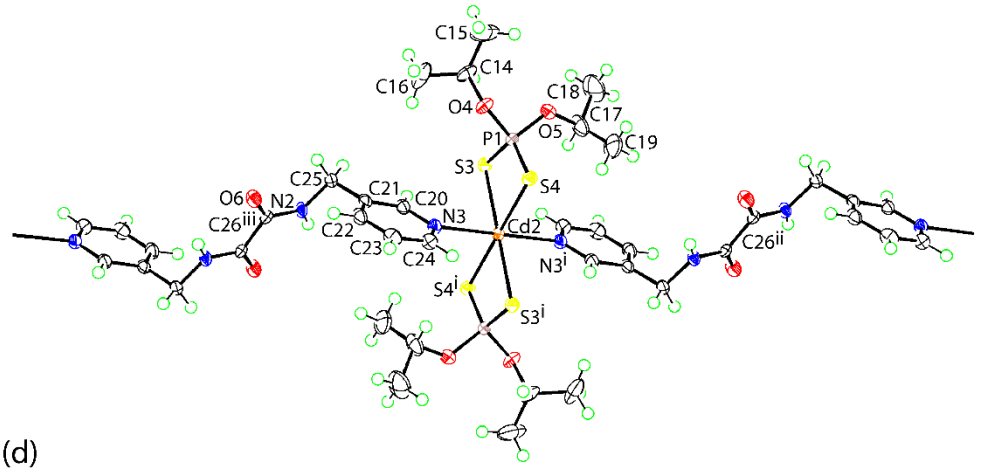
C15
C14
C16
C18
O4
O5
C17
P1
C19
S3
S4
C25
C21
C20
O6
N2
N3
C26iii
C22
Cd2
C26ii
C23
C24
N3i
S4i
S3i

(d)

Fig. 3 The asymmetric-unit, extended to complete the coordination geometry for the cadmium atom and the $^{3}LH_2$ molecules, for (a) **1**, (b) **2**, (c) **3** – first independent molecule (**3**_Cd1) and (d) **3** – second independent molecule (**3**_Cd2), showing atom-labelling schemes and displacement ellipsoids at the 70% probability level. Symmetry operations: (a) i 2-*x*, 1-*y*, 1-*z*; ii *x*, *y*, 1+*z*; iii 2-*x*, 1-*y*, -*z*. (b) i 1-*x*, -*y*, 1-*z*; ii 1+*x*, -1+*y*, -1+*z*; iii -*x*, 1-*y*, 2-*z*. (c) i 1-*x*, 1-*y*, 1-*z*; ii 1+*x*, -1+*y*, -1+*z*; iii -*x*, 2-*y*, 2-*z*. (d) i 1-*x*, 1-*y*, 1-*z*; ii 1+*x*, -1+*y*, -1+*z*; iii -*x*, 2-*y*, 2-*z*.

Table 2 Selected interatomic distances (Å) and mean-plane data (°) about the cadmium centres in **1**-**3**

Parameter	**1**	**2**	**3**_Cd1	**3**_Cd2
Cd–S1	2.7003(4)	2.6716(4)	2.6874(4)	
Cd–S2	2.7053(4)	2.7872(4)	2.7209(4)	
Cd–S3				2.6769(4)
Cd–S4				2.6811(4)
Cd–N1	2.3799(14)	2.3366(13)	2.4145(13)	
Cd–N3				2.4497(12)
Cd···Cd	14.1106(3)	13.8012(7)	15.4749(2)	16.0947(2)
CdS_4/NC_5H_4	89.16(4)	84.62(4)	86.39(4)	86.28(3)
$CdS_4/C_2N_2O_2$	67.81(3)	75.62(4)	64.07(3)	76.17(3)
$NC_5H_4/C_2N_2O_2$	79.08(5)	71.84(4)	64.21(4)	77.47(4)

Side- and end-on views of the resultant coordination polymers are shown in Fig. 4 and again highlights the close relationship between the structures. The pitches of the polymers, defined as the Cd···Cd separation between adjacent cadmium atoms, exhibit no systematic trends with the pitch in **1** being longer, by 0.31 Å, that in **2** but the difference in the pitches for

the two independent chains in **3** differ by 0.62 Å. In each case, the bound pyridyl ring is close to orthogonal to the CdS_4 plane and significant twists are evident in the $^3LH_2$ molecules.

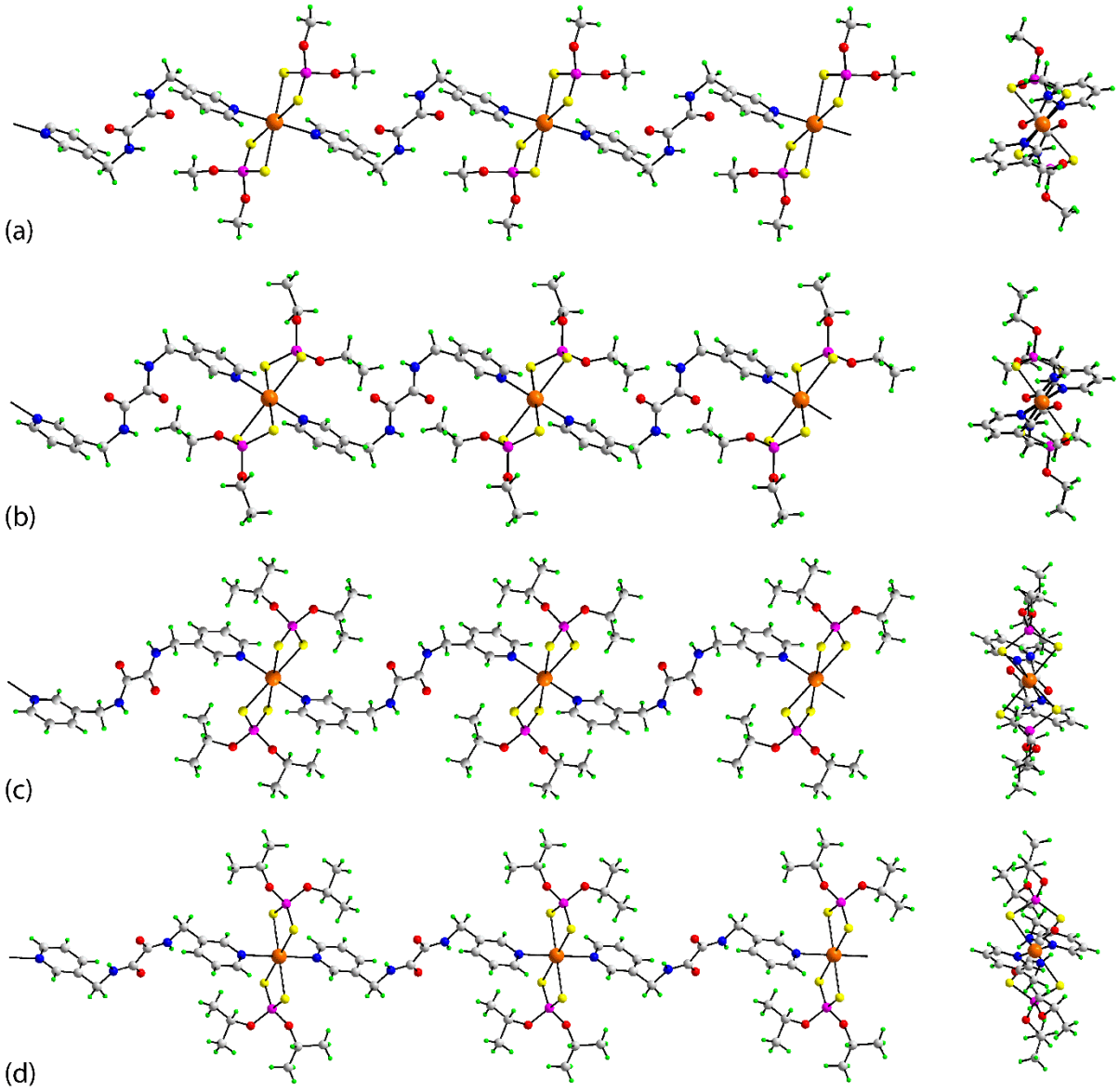

Fig. 4 Side- and end-on views of the one-dimensional coordination polymers formed in (a) **1**, (b) **2**, (c) **3**_Cd1 and (d) **3**_Cd2.

Molecular packing

While conventional hydrogen bonding might be anticipated in the molecular packing of **1**-**3**, owing to the presence of the central oxamide group, this only occurs in the crystal of **3**. Indeed,

three distinctive packing patterns are apparent in the crystals. Based on the point-to-point contacts evident in the crystal of **1**, the molecules assemble into supramolecular layers, parallel to (1 0 1) that stack without directional interactions between them, Fig. 5a. Within the flat layers, amide-N–H···O(methoxy) contacts are complemented by methoxy-C–H···O(amide) interactions leading to non-symmetric, eight-membered {···HNC_2O···HCO} synthons; geometric data characterising the intermolecular contacts for **1**-**3** are collated in Table 3. The {···HNC_2O···HCO} synthon is non-planar with the methyl-C–H component lying well below the plane defined by the remaining six atoms. Within this assembly are rather long π(N1,C3-C7)···π(N1,C3-C7) contacts. However, the slippage between the parallel rings is 1.89 Å so the closest atom-to-atom (C4···C5) contact is 3.577(2) Å; symmetry operation 1-*x*, 2-*y*, 1-*z*.

Table 3 A summary of the geometric parameters (Å, º) characterising the key intermolecular contacts in the crystals of **1**-**3**

Contact	H···B	A···B	A–H···B	Symmetry operation
1				
N2–H1n···O3	2.34(2)	2.7154(19)	106.7(16)	-*x*, 2-*y*, 2-*z*
N2–H1n···O1	2.15(2)	2.953(2)	153.8(18)	1-*x*, 2-*y*, 1-*z*
C1–H1a···O3	2.53	3.335(3)	139	1+*x*, *y*, -1+*z*
Cg(N1,C3-C7)···Cg(N1,C3-C7)	3.9898(10)	0		1-*x*, 2-*y*, 1-*z*
2				
N2–H1n···O3	2.35(2)	2.7104(19)	105.6(13)	-*x*, 1-*y*, 2-*z*
N2–H1n···O2	2.320(12)	3.1017(18)	149.9(17)	-1+*x*, 1+*y*, *z*
C4–H4c···O3	2.54	3.457(2)	157	1-*x*, -*y*, 2-*z*
C10–H10a···Cg(N1,C5-C9)	2.94	3.4461(19)	3.4461(19)	-*x*, 1-*y*, 1-*z*

C8–H8···O1	2.46	3.381(2)	163	1-*x*, 1-*y*, 1-*z*
3				
N2–H1n···O3	2.322(18)	2.7111(18)	107.6(13)	2-*x*, 1-*y*, -*z*
N4–H2n···O6	2.354(19)	2.7105(19)	105.0(13)	1-*x*, 1-*y*, -*z*
N2–H1n···O6	1.968(14)	2.7470(17)	149.6(17)	2-*x*, 1-*y*, -*z*
N4–H2n···O3	1.945(13)	2.7455(17)	152.8(18)	1-*x*, 1-*y*, -*z*
C2–H2b···O5	2.55	3.368(2)	141	1+*x*, *y*, *z*

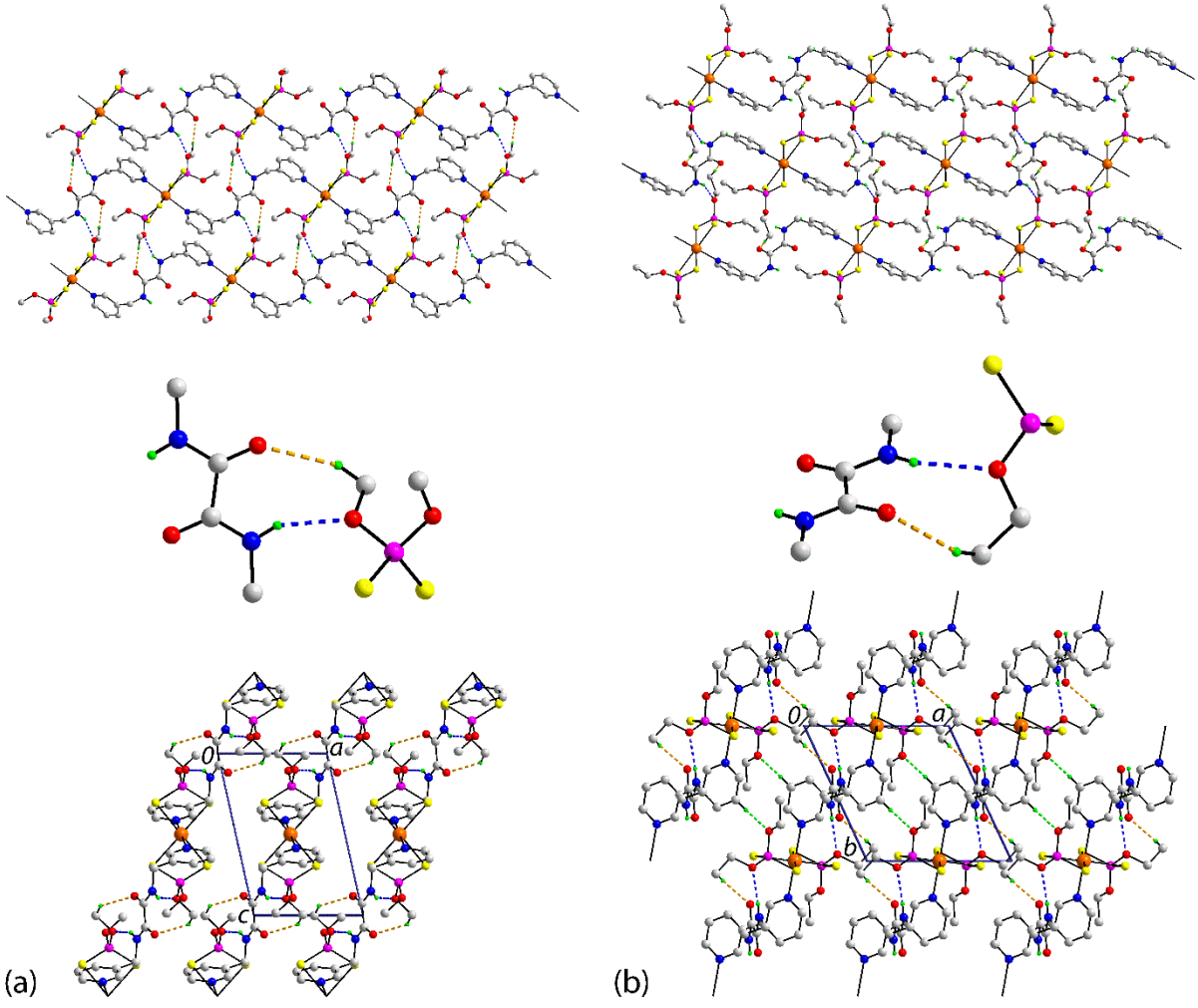

Fig. 5 Supramolecular layer (upper view), new supramolecular synthons and unit-cell contents in the crystals of (a) **1** and (b) **2**. Non-participating hydrogen atoms have been omitted for

clarity. The unit-cell diagrams are shown in projection down the *b* and *c* directions, respectively. The intermolecular contacts are represented by dashed lines: N–H···O (blue), intra-layer C–H···O (orange) and inter-layer C–H···O in **2** (green).

In the crystal of **2**, flat supramolecular layers are also evident as the one-dimensional chains are connected in an analogous fashion to that in **1**, *i.e*. *via* amide-N–H···O(ethoxy) and ethoxy-C–H···O(amide) contacts through a nine-membered {···HNC_2O···HC_2O} synthon, Fig. 5b. As for the related synthon in **1**, the {···HNC_2O···HC_2O} synthon is non-planar with the ethyl-C–C–H atoms lying out of the plane assumed by the remaining six atoms. Within layers are long methylene-C–H···π(pyridyl) and π(N1,C5-C9)···π(N1,C5-C9) contacts. For the latter, the inter-centroid separation is 4.2461(11) Å and the off-set between rings is 2.52 Å with the closest separation of 3.440(2) Å occurring between symmetry-related C6 atoms; symmetry operation -*x*, 1-*y*, 1-*z*. The layers, parallel to (1 1 0), feature pyridyl-C–H···O(ethoxy) interactions between them.

Conventional hydrogen bonding comes to the fore in the packing of **3**. As indicated in Fig. 6a, flat supramolecular tapes are formed through amide-N–H···O(amide) hydrogen bonds occurring on either side of the oxamide residue and non-symmetric, 10-membered {···HNC_2O}$_2$ synthons. The tapes are constructed by alternate independent molecules. The connections leading to the three-dimensional architecture are of the type methyl-C–H···O(*i*-propoxy), Table 3 and Fig. 6b.

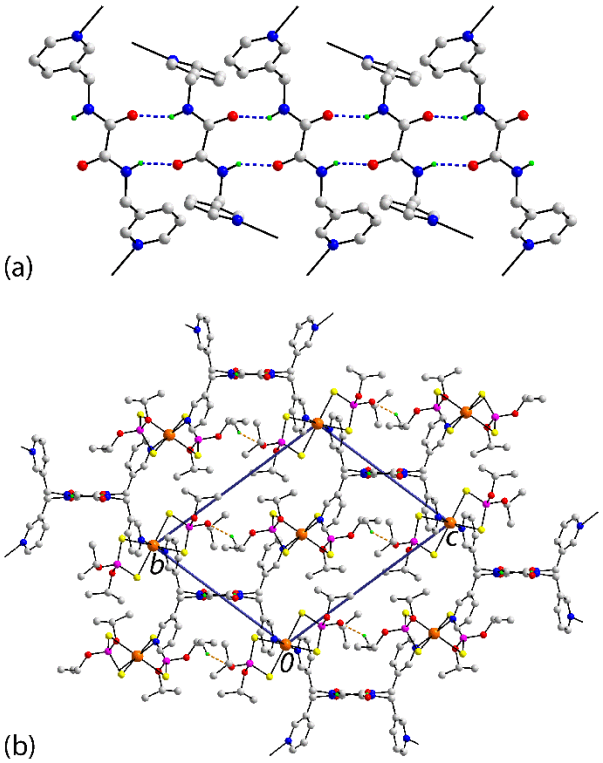

Fig. 6 Supramolecular tape (upper view) and unit-cell contents, view in projection down the *a*-axis, in the crystal of **3**. Non-participating hydrogen atoms have been omitted for clarity. The intermolecular contacts are represented by dashed lines: N–H···O (blue) and C–H···O (orange).

Hirshfeld surface analysis

In order to provide further information on the supramolecular associations in the crystals of **1-3**, an analysis of the calculated Hirshfeld surfaces were conducted by employing *CrystalExplorer21*.[34] In each case, calculations were performed on the {C(O)NCH$_2$C$_5$H$_4$NCd[S$_2$P(O*R*)$_2$]$_2$NC$_5$H$_4$CH$_2$N(O)C} repeat unit, where *R* = Me (**1**), Et (**2**) and *i*-Pr (**3**). The calculations were conducted using wavefunctions at the B3LYP/DGDZVP level of theory. The colour for the d_{norm}-surfaces were scaled between -0.314 (red) and 1.713 a.u. (blue). The brightest red spots on the d_{norm}-Hirshfeld surfaces correspond to the formation of

the covalent bonds between each repeat unit, as shown in Fig. 7 for **1**; see ESI† Fig. 7. The key interatomic parameters identified from the analyses are listed in Table 4.

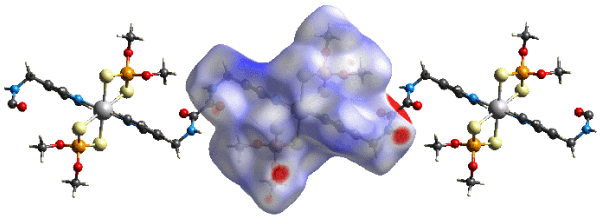

Fig. 7. View of the d_{norm}-Hirshfeld surface for **1** highlighting the covalent bonds between each repeat unit as large bright red spots.

Table 4 Summary of short interatomic contacts (Å) in **1**-**3**.[a]

Contact	Distance	Symmetry operation
1		
Intralayer		
N2–H1n···O1[b]	2.02	-*x*+1, -*y*+2, -*z*+1
C1–H1a···O3[b]	2.45	*x*+1, *y*, *z*-1
Cg(N1,C3-C7)···*Cg*(N1,C3-C7)[b]		-*x*+1, -*y*+2, -*z*+1
Interlayer		
O2···O2	1.81	-*x*+1, -*y*+1, -*z*
2		
Intralayer		
N2–H1n···O2[b]	2.20	-1+*x*, 1+*y*, *z*
C4–H4c···O3[b]	2.94	-*x*, 1-*y*, 2-*z*
C10–H10a···Cg(N1,C5-C9)[b]		1-*x*, 1-*y*, 1-*z*

Interlayer		
C8–H8···O1[b]	2.33	1-*x*, 1-*y*, 1-*z*
3		
N2–H1n···O6[b]	1.84	2-*x*, 1-*y*, -*z*
N4–H2n···O3[b]	1.82	2-*x*, 1-*y*, -*z*
C2–H2b···O5[b]	2.47	1+*x*. *y*, *z*
C9–H9···O6	2.50	2-*x*, 1-*y*, -*z*
C12···S4	3.43	1-*x*+, 2-*y*, -*z*
H12b···H20	2.15	1-*x*, 2-*y*, -*z*

Note: (a) The inter-atomic distances are measured in *Crystal Explorer21* whereby the X–H bond lengths are adjusted to their neutron values; (b) these interactions correspond to the interactions listed in Table 3.

In the views of Fig. 8, the red spots on the d_{norm}-Hirshfeld surfaces of **1** and **2** reflect the amide-N–H···O(alkoxy) and alkoxy-C–H···O(amide) interactions. These interactions connect the molecules into supramolecular layers.

The individual π···π and C–H···π interactions as discussed above were not manifested on the d_{norm}-Hirshfeld surfaces of **1** and **2**. However, the π···π interaction appears as a flat surface on the curvedness Hirshfeld surface of **1**, Fig. 9a, and the C–H···π interaction appears as a red concave and blue bump regions on the shape index Hirshfeld surface of **2**, Fig. 9b.

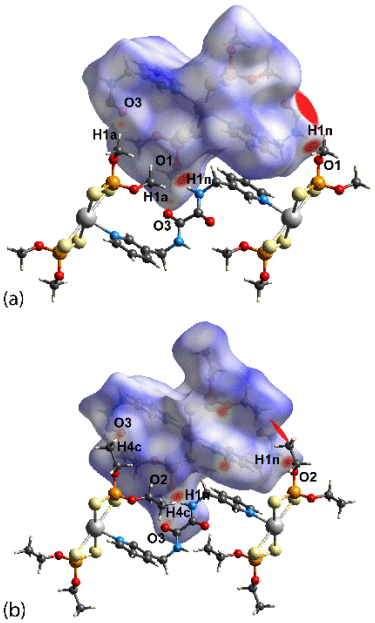

Fig. 8. Views of the d_{norm}-Hirshfeld surfaces for (a) **1** and (b) **2**, highlighting the amide-N–H···O(alkoxy) and alkoxy-C–H···O(amide) interactions.

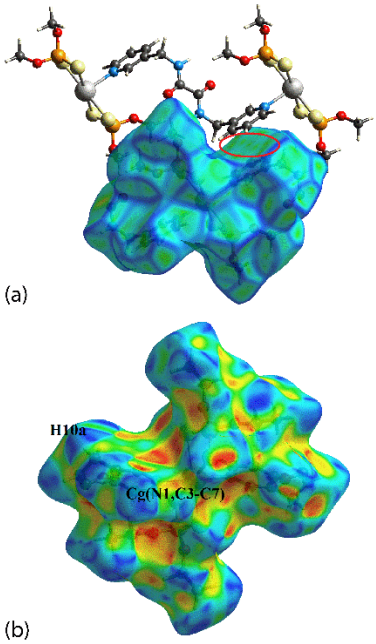

Fig. 9. Views of the Hirshfeld surface mapped over (a) curvedness and (b) the shape index property highlighting the intermolecular π···π and C–H···π interaction for **1** and **2**, respectively.

Between the supramolecular layers of **1**, O2···O2 short contacts with a distance of 0.07 Å shorter than the sum of their van der Waals radii,[32] was observed on the d_{norm}-Hirshfeld surface, Fig. 10a. Whereas, the inter-layer pyridyl-C–H···O(ethoxy) interaction in **2** emerged as red spot near the ethoxy-O1 and pyridyl-H8 atoms, Fig. 10b.

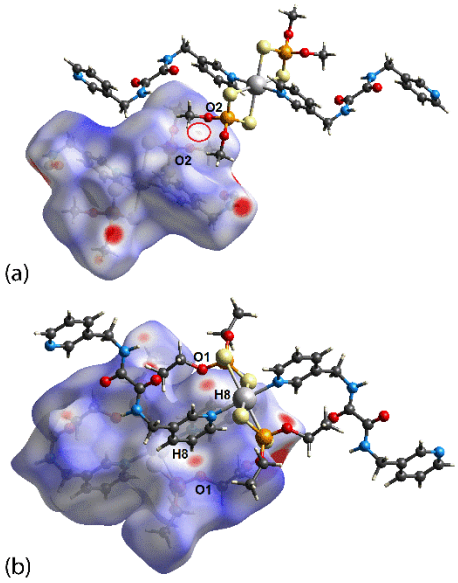

Fig. 10. Views of the d_{norm}-Hirshfeld surface for (a) **1** and (b) **2**, highlighting the short intermolecular O···O and C–H···O interaction, respectively.

Attention is now directed towards the two independent repeat units of **3**, *i.e.* **3**_Cd1 and **3**_Cd2. In the views of Fig 11, the bright-red spots appearing near the amide (H1n, H2n, O3 and O6), methyl (H2b) and *i*-propoxy (O5) atoms correspond to the conventional amide-N–H···O(amide) hydrogen bonds, leading to the tape, and the methyl-C–H···O(*i*-propoxy) interaction. Meanwhile, the weak C12···S4 and H12b···H20 short contacts (Table 4) are observed as faint-red spots near the methylene (C12, H12b), sulphur (S4) and pyridyl (H20) atoms, ESI† Fig. 8. In addition, the weak pyridyl-C9–H9···O6(amide) interaction was also observed as faint-red spot on d_{norm}-Hirshfeld surfaces of **3**, ESI† Fig. 8.

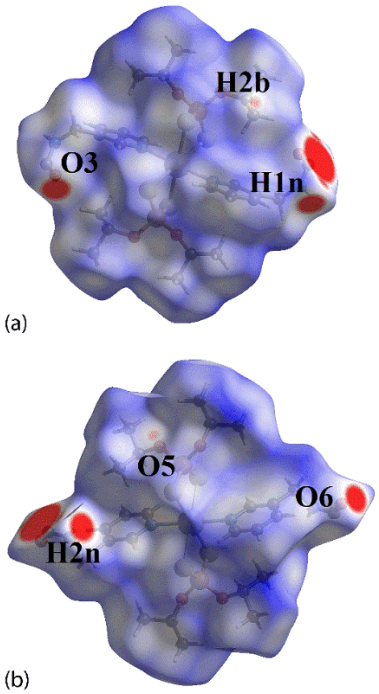

Fig. 11. Views of the d_{norm}-Hirshfeld surface of **3** for the (a) Cd1- and (b) Cd2-containing repeat units, highlighting the intermolecular N–H···O and C–H···O interactions as notable red spots.

In order to determine the contributions to the surface contacts for each repeat unit in **1-3**, the overall and delineated (H···H, H···S/S···H, H···O/O···H and H···C/C···H) two-dimensional fingerprint plots were generated; these are illustrated in ESI† Fig. 9. The percentage contributions of the delineated contacts are tabulated in Table 5. As the greatest contributor to all the Hirshfeld surfaces, the H···H contacts contributed a minimum of 38.3% to the surface of **1** and a maximum of 60.4% to the surface of **3**_Cd1. The systematic trend is consistent with the increasing hydrogen atom content in the order **1** < **2** < **3**. Owing to the presence of a H···H short contact between both repeat units of **3**, the feature due to these contacts is a sharp peak tipped at $d_e = d_i \approx 2.2$ Å. Whereas, the H···H contacts for **1** and **2** are shown as rounded peaks tipped at $d_e = d_i \approx 2.4$ Å.

Table 5 Percentage contributions of inter-atomic contacts to the Hirshfeld surfaces of **1**, **2**, **3**_Cd1 and **3**_Cd2.

Contact	**1**	**2**	**3_Cd1**	**3_Cd2**
H···H	38.3	51.0	60.4	59.2
H···S/S···H	21.3	19.0	15.4	14.2
H···O/O···H	20.9	16.3	16.3	14.3
H···C/C···H	11.6	8.0	4.6	7.5
C···C	4.1	2.9	2.0	2.9
H···N/N···H	3.1	2.3	1.0	1.5
N···S/S···N	0.1	0.0	0.3	0.3
H···P/P···H	0.1	0.3	0.0	0.0
O···O	0.4	0.1	0.0	0.0
S···S	0.1	0.1	0.0	0.0
S···O/O···S	0.0	0.0	0.0	0.1

The next most significant percentage contributors to the Hirshfeld surfaces are H···S/S···H contacts which decreased from 21.3 to 14.2% to the overall surface for the respective repeat units of **1** through **3**. The H···S/S···H contacts appear as distinctive forceps-like peaks tipped at $d_e + d_i \approx 3.0$ Å, where this distance is around the sum of the respective van der Waals radii.[32] Although, N–H···O and C–H···O contacts are present in the molecular packing of all compounds, H···O/O···H contacts only contributed 20.9 to 14.3% to the overall surface, following the trend for the H···S/S···H contacts. The crystal of **3** has stronger interatomic H···O/O···H interactions as indicated by the pseudo symmetric spikes tipped at $d_e + d_i \approx 1.8$ Å, as compared to **1** and **2** which tipped at $d_e + d_i \approx 2.0$ Å. The H···C/C···H contacts, appear as wing-like peaks tipped at $d_e + d_i \approx 2.8$ Å and contributed 4.6-11.6% to the overall

Hirshfeld surface, there being no systematic trends. The percentage contributions for other interatomic contacts in **1**-**3** are listed in Table 5. These contacts have only small effects effect on the molecular packing as their accumulated contribution is below 8% in each crystal.

Interaction energies

The pairwise interaction energies of **1-3** were calculated by employing the DGDZVP basis set with the B3LYP function.[34] The total energy comprises four components: *i.e.* the sum of the electrostatic (E_{ele}), polarization (E_{pol}), dispersion (E_{dis}) and exchange-repulsion (E_{rep}) energy terms and were calculated with *CrystalExplorer21*.[34] The individual energy components as well as the total interaction energies are collated in Table 6; the scale factors for the four energy terms are 1.057, 0.740, 0.871 and 0.618, respectively. As foreseen, the dispersive component makes the major contribution to the interaction energies in the intra-layer region of **1** and **2**, owing to the absence of conventional hydrogen bonding interactions. The stabilisation energies in the inter-layer region for **1** are also dominated by the E_{dis} component (E_{dis} = -63.2 kJ/mol) which incorporates the short O···O contacts. For the inter-layer C8–H8···O1 interaction in **2**, mentioned above, there are almost equal contributions from E_{ele} and E_{dis}, Table 6. By contrast, for **3**, the E_{ele} component makes a slightly greater contribution to the stabilisation energies (E_{ele} = -114.5 kJ/mol *cf.* E_{dis} = -109.6 kJ/mol), owing to the presence of conventional amide-N–H···O (amide) hydrogen bonds.

Table 6. Calculated interaction energies (kJ/mol) in the crystals of **1**-**3**.

Contact	R (Å)	E_{ele}	E_{pol}	E_{dis}	E_{rep}	E_{tot}
1						
Intra-layer region						
N2–H1n···O1 +	9.64	-46.1	-18.3	-81.8	53.9	-100.2

C1–H1a···O3 + Cg(N1,C3-C7)···Cg(N1,C3-C7)						
Inter-layer region						
O2···O2	10.45	-3.5	-4.1	-63.2	28.6	-44.1
2						
Intra-layer region						
N2–H1n···O1 + C4–H4c···O3 + C10–H10a···Cg(N1,C5-C9)	9.70	-115.1	-27.6	-118.2	149.6	-149.4
Inter-layer region						
C8–H8···O1	9.21	-56.8	-11.2	-60.8	80.3	-71.7
3						
N2–H1n···O6 + N4–H2n···O3 + C2–H2b···O5 + C9–H9···O6 + C12···S4 + H12b···H20	11.16	-114.5	-25.8	-109.6	169.5	-130.8

It is not possible to delineate the contributions made to the overall energies by individual contacts as intermolecular contacts do not operate in isolation but are operating in concert with cooperating contacts.[35] However, the relatively high energies associated with the amide-N–H···O(alkoxy) and alkoxy-C–H···O(amide) contacts, incorporating other contacts,

are noted: indeed, the maximum energy is found for crystal **2**, *i.e*. even greater than the sum of all interaction energies calculated for **3**, Table 6.

Literature survey

In the quest to ascertain the possible reason(s) for the disparity in the key elements of the molecular packing in **1** and **2** on the one hand, and that in **3**, searches were made of the crystallographic literature employing the Cambridge Structural Database[36] (CSD version 5.42 plus two updates) was conducted employing ConQuest (version 2021.1.0).[37]

Initially, metal complexes of $^3LH_2$ were extracted revealing 13 structures, consistent with the comment in the *Introduction* that despite the opportunities these molecules hold for supramolecular assembly, their study is still in its infancy. Data for the literature "hits" and for **1**-**3** are included in Table 7. Of the 16 examples, only four feature the supramolecular tapes constructed *via* concatenated $\{\cdots HNCCO\}_2$ synthons. Clearly, other considerations come into play in the 12 remaining structures to preclude the formation of the tapes. In fact, two of the remaining examples do form amide-N–H···O(amide) contacts in their crystals. In the co-crystal, $[Mn(1,3\text{-}O_2CC_6H_3ICO_2)(^3LH_2)]_n$, $n(^3LH_2)$,[39] supramolecular tapes *via* concatenated $\{\cdots HNCCO\}_2$ synthons are formed but these occur between the co-formers, *i.e*. the $^3LH_2$ co-formers literally insert themselves within the tape that might have been formed by the coordinated $^3LH_2$ molecules, a phenomenon classified as masked synthons.[46] In the binuclear species, $(Ph_2PCH_2PPh_2)Pd(^3LH_2)_2Pd(Ph_2PCH_2PPh_2)$,[40] an endocyclic $\{\cdots HNC_2O\}_2$ synthon connects the coordinated $^3LH_2$ molecules with the exocyclic amide groups engaged in amide-N–H···O(triflate) and phenyl-C–H···O(amide) connections. The latter observation sets the tone of the remaining structures whereby other hydrogen bonds are evident.

Table 7 Summary of available structurally characterised metal complexes of $^{3}LH_2$.

Composition	Amide tape	Amide supramolecular association	CSD Refcode	Reference
$[Ag(^{3}LH_2)]_n$, n(NO_3)	yes	amide-N–H···O(amide)	NOQSUH	5
$[Ag(^{3}LH_2)]_n$, n(BF_4)	yes	amide-N–H···O(amide)	NOQTAO	5
$\{Zn[S_2CN(i\text{-}Pr)_2]_2\}_2(^{3}LH_2)$	yes	amide-N–H···O(amide)	HECLOT	38
$\{Cd[S_2P(O\text{-}i\text{-}Pr)_2]_2(^{3}LH_2)\}_n$ (**3**)	yes	amide-N–H···O(amide)	–	This work
$[Mn(1,3\text{-}O_2CC_6H_3ICO_2)(^{3}LH_2)]_n$, n($^{3}LH_2$)	no	amide-N–H···O(amide)	IPEFER	39
$(Ph_2PCH_2PPh_2)Pd(^{3}LH_2)_2Pd(Ph_2PCH_2PPh_2)$, 4($CF_3CO_2$), 2($Me_2C$=O)			XACDEL	40
	no	amide-N–H···O(amide); amide-N–H···O(triflate) & phenyl-C–H···O(amide)		
$\{Cd[S_2P(OMe)_2]_2(^{3}LH_2)\}_n$ (**1**)	no	amide-N–H···O(methoxy) methoxy-C–H···O(amide)	–	This work
$\{Cd[S_2P(OEt)_2]_2(^{3}LH_2)\}_n$ (**2**)	no	amide-N–H···O(ethoxy) ethoxy-C–H···O(amide)	–	This work

$[Co_2(O_2C_2O_2)_2(^3LH_2)_2]_n$	no	amide-N–H···O(oxalate) & methylene-C–H···O(amide)	WOJSOF	41
$\{Au_4(Ph_2PC_{10}H_6\text{-}C_{10}H_6PPh_2)_2(^3LH_2)_2\}_n$, $4n(CF_3CO_2)$, $5n(CH_2Cl_2)$	no	2 × amide-N–H···O(carboxylate) & 2 × DCM–H···O(amide)	OJIMOL	42
$[Cu(^3LH_2)Br]_n$, $n(Br)$, $2n(H_2O)$	no	amide-N–H···O(water)	CIYZUG	43
$[Cu_2$(4-amino-3-carboxylatobenzene-1-sulfonate$)_2(^3LH_2)_2(OH_2)_2]_n$, $2n(H_2O)$	no	amide-N–H···O(water) water-O–H···O(amide)	OMEMOL	44
$[Zn(S_2CNMe_2)_2]_2(^3LH_2)$, 2DMF	no	amide-N–H···O(DMF) & DMF-C–H···O(amide)	HECLIN	38
$[Zn$(phthalocyaninato$)]_2(^3LH_2)$, 4DMF	no	amide-N–H···O(DMF)	IXUDAH	45
$\{Zn[S_2CN(Me)CH_2CH_2OH]_2(^3LH_2)\}_n$	no	hydroxy-O–H···O(amide)	NUWRIH	9
$[Zn$(5,10,15,20-tetraphenylporphyrinato$)]_2(^3LH_2)$, $2(ClCH_2CH_2Cl)$, $4H_2O$	no	none	IXUCUA	45

In **1** and **2**, by amide-N–H···O(alkoxy) interactions, and $[Co_2(O_2C_2O_2)_2(^3LH_2)_2]_n$,[41] by amide-N–H···O(oxalate) contacts, close contacts are made with other residues within the one-dimensional coordination polymers; the amide-O atoms form contacts with C-bound H atoms. In $\{Au_4(Ph_2PC_{10}H_6\text{-}C_{10}H_6PPh_2)_2(^3LH_2)_2\}_n$,[42] amide-to-amide synthons are precluded owing to amide-N–H···O(carboxylate) hydrogen bonding by each of the independent $^3LH_2$ molecules. Hydrogen bonding of the type amide-N–H···O(water) comes to the fore in each of $[Cu(^3LH_2)Br]_n$ (ref. 43) and $[Cu_2$(4-amino-3-carboxylatobenzene-1-sulfonate$)_2(^3LH_2)_2(OH_2)_2]_n$.[44] Even lattice DMF can disrupt the formation of the amide synthon by forming amide-N–H···O(DMF) contacts, as in the binuclear species $[Zn(S_2CNMe_2)_2]_2(^3LH_2)$[38] and [Zn(phthalocyaninato)$]_2(^3LH_2)$.[45] In the crystal of $\{Zn[S_2CN(Me)CH_2CH_2OH]_2(^3LH_2)\}_n$ (ref. 9), conventional hydroxy-O–H···O(amide) hydrogen bonding involving the amide-O atom disrupts the formation of the $\{\cdots HNCCO\}_2$ synthon. Finally, an example exists, *i.e.* [Zn(5,10,15,20-tetraphenylporphyrinato)$]_2(^3LH_2)$,[45] where neither of the amide-N–H or amide-O atoms participates in recognisable contacts, as the amide group is enclosed within an intramolecular, hydrophobic pocket.

A survey of the CSD was then conducted where the number of structures containing the oxalamide core, *i.e.* C–N(H)C(=O)–C(=O)N(H)–C. For all-organic molecules, this returned 306 "hits" and of these, 112 formed tapes in their crystals; for organometallic species there were only eight examples where tape formation was apparent out of 147 "hits". The percentage adoption by organic and organometallic molecules, *i.e.* 37% *vs* 5%. Thus, supramolecular tape formation mediated by $\{\cdots HNC_2O\}_2$ synthons is clearly less likely in organometallic crystals; the value of 37% is higher than the 24% adoption rate of eight-membered $\{\cdots HNCO\}_2$ synthons in all-organic crystals of monofunctional amides.[47]

Next, attention focussed on the propensity of formation of the eight-, $\{\cdots HNC_2O\cdots HCO\}$, and nine-membered, $\{\cdots HNC_2O\cdots HC_2O\}$, synthons formed in the

crystal of **1** and **2**, respectively. A search for analogous synthons in the CSD, gave no "hits". There were seven structures having both (O=)C–C–N(H)–C and P–O–CH where the {···HNC_2O···HCO} synthon could potentially form but did not; each structure was organometallic. A similar search to evaluate possible structures having the residues to potentially form an analogous synthon to that observed in **2**, retrieved the same seven "hits".

Overview

The crucial structure-directing differences in the crystals of **1**-**3** relate to the usurping of the anticipated edge-shared {···HNC_2O}$_2$ synthon, as observed in **3**, with {···HNC_2O···HCO} and {···HNC_2O···HC_2O} synthons seen instead in the molecular packing of in **1** and **2**, respectively. It turns out supramolecular tapes are not prevalent in the crystals of related $^3LH_2$ complexes nor in general. There are no literature precedents for the aforementioned synthons in **1** and **2**. The disruption of the {···HNC_2O}$_2$ synthon precluding the formation of tapes can arise owing to intra- and inter-molecular contacts between the amide-N–H and a variety of acceptor atoms, usually oxygen, in ligands, counter-ions and solvent molecules so the adoption of the {···HNC_2O}$_2$ synthon leading to tapes in crystals of metal complexes must be regarded fickle and subject to other factors. In terms of the densities of the crystals, Table 1, these follow the expected trends, *i.e.* relating to the size of the *R* groups, and the packing efficiencies, calculated in PLATON,[32] decrease in the order 70.8, 68.8 and 66.2% for **1**-**3**, respectively, again according to expectation. The question then arises, why is there a difference in the molecular packing in terms of supramolecular synthon exchange.

In terms of chemistry, the obvious difference between **1**-**3**, relates to the *R* groups in {Cd[$S_2P(OR)_2$]$_2$($^3LH_2$)}$_n$. One scenario is the smaller *R* = Me and Et groups, having a greater inductive effect, than *R* = *i*-Pr, could activate the P-bound oxygen atoms to encourage the formation of the new {···HNC_2O···HCO} and {···HNC_2O···HC_2O} synthons; the *R* = *i*-Pr

group, having a smaller inductive effect, does not exert a similar effect. A second explanation rests with the relative steric bulk of the *R* groups, known to be important for 1,1-dithiolate, including dithiophosphate, complexes of the zinc-triad elements.[14-16,22,23] The bulk of the *R* = *i*-Pr group precludes the formation of analogous synthons observed in **1** and **2** and hence, the supramolecular tape is observed in the crystal of **3**.

Conclusions

A series of linear one-dimensional coordination polymers formulated as $\{Cd[S_2P(OR)_2]_2(^3LH_2)\}_n$, for *R* = Me (**1**), Et (**2**) and *i*-Pr (**3**), has been synthesised and characterised by a variety of spectroscopic and physiochemical techniques, and their supramolecular association evaluated by a broad range of computational methods. The supramolecular association is dependent on the nature of *R* in that the smaller groups, each with a greater inductive effect, in **1** and **2** enable and promote the formation of unprecedented $\{\cdots HNC_2O\cdots HCO\}$ and $\{\cdots HNC_2O\cdots HC_2O\}$ synthons, respectively, leading to two-dimensional arrays. By contrast, the larger *i*-Pr group, with a reduced inductive effect, precludes the formation of the analogous synthons enabling the formation of supramolecular tapes mediated by $\{\cdots HNC_2O\}_2$ synthons in the crystal of **3**.

Conflicts of interest

The authors declare no competing financial interest.

Acknowledgements

The authors gratefully acknowledge Sunway University Sdn Bhd (Grant numbers GRTIN-IRG-01-2021, GRTIN-IRG-14-2021 and GRTIN-IRG-18-2021) for support of this research.

References

1. J. C. MacDonald and G. M. Whitesides, *Chem. Rev*., 1994, **94**, 2383-2420.
2. T. R. Shattock, K. K. Arora, P. Vishweshwar and M. J. Zaworotko, *Cryst. Growth Des*., 2008, **8**, 4533–4545.
3. S. R. Batten, N. R. Champness, X. M. Chen, J. Garcia-Martinez, S. Kitagawa, L. Öhrström, M. O'Keeffe, M. P. Suh and J. Reedijk, *CrystEngComm*, 2012, **14**, 3001–3004.
4. E. R. T. Tiekink, Crystal chemistry of the isomeric N,N'-bis(pyridin-n-ylmethyl)-ethanediamides, n = 2, 3 or 4 in E. R. T. Tiekink and J. Zukerman-Schpector (Eds), *Multi-Component Crystals. Synthesis, Concepts, Function*, De Gruyter, Singapore, 2017.
5. C. L. Schauer, E. Matwey, F. W. Fowler and J. W. Lauher, *J. Am. Chem. Soc*., 1997, **119**, 10245–10246.
6. T. L. Nguyen, A. Scott, B. Dinkelmeyer, F. W. Fowler and J. W. Lauher, *New J. Chem.*, 1998, **22**, 129–135.
7. T. L. Nguyen, F. W. Fowler and J. W. Lauher, *J. Am. Chem. Soc*., 2001, **123**, 11057–11064.
8. N. S. Goroff, S. M. Curtis, J. A. Webb, F. W. Fowler and J. W. Lauher, *Org. Lett*., 2005, **7**, 1891–1893.
9. P. Poplaukhin and E. R. T. Tiekink, *CrystEngComm*, 2010, **12**, 1302–1306.
10. M. M. Jotani, J. Zukerman-Schpector, L. Sousa Madureira, P. Poplaukhin, H. D. Arman, T. Miller and E. R. T. Tiekink, *Z. Kristallogr. Cryst. Mater*., 2016, **231**, 415–425.
11. G.-H. Lee and H. T. Wang, *Acta Crystallogr., Sect. C: Cryst. Struct. Commun*., 2007, **63**, m216–219.
12. G. -H. Lee, *Acta Crystallogr., Sect. C: Cryst. Struct. Commun*., 2010, **66**, o241–244.

13. J. Zukerman-Schpector, L. Sousa Madureira, P. Poplaukhin, H. D. Arman, T. Miller and E. R. T. Tiekink , *Z. Kristallogr. Cryst. Mater*., 2015, **230**, 531–541.
14. E. R. T. Tiekink, *CrystEngComm*, 2003, **5**, 101–113.
15. E. R. T. Tiekink, *Crystals*, 2018, **8**, article no. 292.
16. E. R. T. Tiekink, *Crystals*, 2018, **8**, article no. 18.
17. H. D. Arman, P. Poplaukhin and E. R. T. Tiekink, *Acta Crystallogr., Sect. E: Cryst. Commun*., 2017, **73**, 1501–1507.
18. H. D. Arman, P. Poplaukhin and E. R. T. Tiekink, *Z. Kristallogr.-New Cryst. Struct*., 2018, **233**, 159–161.
19. Y. S. Tan, H. Z. Chun, M. M. Jotani and E. R. T. Tiekink, *Z. Kristallogr. Cryst. Mater*., 2019, **234**, 165–175,
20. Y. S. Tan and E. R. T. Tiekink, *Z. Kristallogr. - New Cryst. Struct*., 2020, **235**, 327–329.
21. L. A. Glinskaya, V. G. Shchukin, R. F. Klevtsova, A. N. Mazhara and S. V. Larionov, *J. Struct. Chem*., 2000, **41**, 632–639.
22. C. S. Lai, S. Liu and E. R. T. Tiekink, *CrystEngComm*, 2004, **6**, 221–226.
23. C. S. Lai and E. R. T. Tiekink, *CrystEngComm*, 2004, **6**, 593–605.
24. Y. S. Tan, A. L. Sudlow, K. C. Molloy, Y. Morishima, K. Fujisawa, W. J. Jackson, W. Henderson, S. N. Bt. A. Halim, S. W. Ng and E. R. T. Tiekink, *Cryst. Growth Des.*, 2013, **13**, 3046–3056.
25. M. M. Jotani, Y. S. Tan and E. R. T. Tiekink, *Z. Kristallogr. – Cryst. Mater.*, 2016, **231**, 403–413.
26. Y. S. Tan, A. Otero-de-la-Roza, M. M. Jotani and E. R. T. Tiekink, *Cryst. Growth Des.,* 2020, **20**, 3272–3283.
27. S. L. Lawton and G. T. Kokotailo, *Inorg. Chem*., 1969, **8**, 2410–2421.

28. Rigaku Oxford Diffraction, CrysAlis PRO, Yarnton, Oxfordshire, England (2017).

29. G. M. Sheldrick, *Acta Crystallogr., Sect. A: Found. Crystallogr*., 2008, **64**, 112–122.

30. G. M. Sheldrick, *Acta Crystallogr., Sect. C: Struct. Chem*., 2015, **71**, 3–8.

31. L. J. Farrugia, *J. Appl. Crystallogr*., 2012, **45**, 849–854.

32. A. L. Spek, *Acta Crystallogr., Sect. E: Crystallogr. Commun*., 2020, **76**, 1–11.

33. K. Brandenburg, DIAMOND, Crystal Impact GbR, Bonn, Germany, 2006.

34. P. R. Spackman, M. J. Turner, J. J. McKinnon, S. K. Wolff, D. J. Grimwood, D. Jayatilaka and M. A. Spackman, *J. Appl. Cryst*., 2021, **54**, 1006–1011.

35. A. S. Mahadeviand and G. N. Sastry, *Chem. Rev*., 2016, **116**, 2775–2825.

36. C. R. Groom, I. J. Bruno, M. P. Lightfoot and S. C. Ward, *Acta Crystallogr., Sect. B: Struct. Sci., Cryst. Eng. Mater*., 2016, **72**, 171–179.

37. I. J. Bruno, J. C. Cole, P. R. Edgington, M. Kessler, C. F. Macrae, P. McCabe, J. Pearson and R. Taylor, *Acta Crystallogr., Sect. B: Struct. Sci., Cryst. Eng. Mater*., 2002, **58**, 389–397.

38. H. D. Arman, P. Poplaukhin and E. R. T. Tiekink, *Acta Crystallogr., Sect. E: Cryst. Commun*., 2017, **73**, 1501–1507.

39. J.-l. Zhu, P. Zhu, J. Mei, J. Xie, J. Guan and K.-L. Zhang, *Polyhedron*, 2021, **200**, 115139.

40. Z. Qin, M. C. Jennings and R. J. Puddephatt, *Inorg. Chem*., 2003, **42**, 1956–1965.

41. H. Zou and Y. Qi, *Acta Crystallogr., Sect. E: Struct. Rep. Online*, 2014, **70**, m307–m308.

42. C. A. Wheaton and R. J. Puddephatt, *Polyhedron*, 2016, **120**, 88–95.

43. Q. Zeng, M. Li, D. Wu, S. Lei, C. Liu, L. Piao, Y. Yang, S. An and C. Wang, *Cryst. Growth Des*., 2008, **8**, 869–876.

44. J.-L. Zhu, P. Zhu, H.-T. Chen, M. Yan and K.-L. Zhang, *CrystEngComm*, 2021, **23**, 1929–1941.

45. X. Li, X. He, Y. Chen, X. Fan and Q. Zeng, *J. Mol. Struct.*, 2011, **1002**, 145–150.

46. J. R. G. Sander, D.-K. Bučar, R. F.Henry, B. N. Giangiorgi, G. G. Z. Zhang and L. R. MacGillivray, *CrystEngComm.*, 2013, **15**, 4816–4822.

47. F. H. Allen, W. D. S. Motherwell, P. R. Raithby, G. P. Shields and R. Taylor, *New J. Chem*., 1999, **23**, 25−34.